JCTC Journal of Chemical Theory and Computation

# Quantum Cluster Equilibrium Theory Applied in Hydrogen Bond Number Studies of Water. 1. Assessment of the Quantum Cluster Equilibrium Model for Liquid Water

S. B. C. Lehmann, C. Spickermann, and B. Kirchner*

*Wilhelm-Ostwald Institute of Physical and Theoretical Chemistry, University of Leipzig, Linnéstrasse 2, D-04103 Leipzig, Germany*

Received July 31, 2008

**Abstract:** Different cluster sets containing only 2-fold coordinated water, 2- and 3-fold coordinated water, and 2-fold, 3-fold, and tetrahedrally coordinated water molecules were investigated by applying second-order Møller−Plesset perturbation theory and density functional theory based on generalized gradient approximation functionals in the framework of the quantum cluster equilibrium theory. We found an improvement of the calculated isobars at low temperatures if tetrahedrally coordinated water molecules were included in the set of 2-fold hydrogen-bonded clusters. This was also reflected in a reduced parameter for the intercluster interaction. If all parameters were kept constant and only the electronic structure methods were varied, large basis set dependencies in the liquid state for the density functional theory results were found. The behavior of the intercluster parameter was also examined for the case that cooperative effects were neglected. The values were 3 times as large as in the calculations including the total electronic structure. Furthermore, these effects are more severe in the tetrahedrally coordinated clusters. Different populations were considered, one weighted by the total number of clusters and one depending on the monomers.

## 1. Introduction

Calculating thermodynamic properties of condensed phases gives rise to substantial problems in computational chemistry, especially if systems exhibiting complicated electronic structures are involved; see e.g., refs 1 and 2. In general, these systems have to be treated in terms of quantum chemical *first-principles* methods, e.g., ab initio molecular dynamics (AIMD) simulations, from which reliable thermodynamic data for systems with many degrees of freedom are only obtained under very large computational efforts, if at all. The quantum cluster equilibrium (QCE) model circumvents these sampling problems of the phase space by decomposing the condensed phase into a thermodynamic equilibrium of distinct cluster structures, which in the zeroth approximation are treated as indistinguishable, noninteracting particles.[3,4] For this noninteracting cluster phase an analytical, ideal-gas-like partition function is available, which gives direct access to the thermodynamics of the system. Two central corrections are introduced to this ideal "cluster gas" to account for the special conditions at liquid-phase densities, namely, the reduced free volume of translation and the interaction between different clusters, which are adjustable by means of two scaling parameters. The cluster structures and corresponding properties are obtained from static quantum chemical calculations, in which sophisticated ab initio methods are applicable, thus enabling the treatment of demanding electronic structures on the cluster level. The intercluster interaction is realized in the present model according to a nonlocal, van der Waals-like mean field potential, which in principle could be replaced by more advanced expressions. In this way the QCE approach introduces ab initio quantum chemistry including correlated electronic structure methods to the condensed phase. A recent example for this procedure is the determination of the vaporization entropy of water, which for the first time has

* Corresponding author phone: 493419736401; fax: 493419736399; e-mail: bkirchner@uni-leipzig.de.

10.1021/ct800310a CCC: $40.75 
Published on Web 05/13/2009

been calculated on the basis of correlated electronic structure methods.[5] Besides the accurate treatment of electron correlation, nuclear quantum effects are within the scope of the model in terms of ab initio cluster frequency analyses as well. However, the maybe most important point concerning the investigation of highly associated liquids is the inclusion of cooperative effects, which have been demonstrated to be of high importance for the accurate calculation of various thermodynamic properties for the liquid water phase.[5,6]

The QCE model already proved to be applicable to a variety of associated liquids, the most prominent of which is pure water. The first QCE application already pointed out that in the case of water generic structural patterns (so-called "cluster motifs") are more important than special cluster sizes and geometries, and additional studies demonstrated that the model is capable of reproducing large parts of water's phase diagram at least qualitatively, including the triple point and a phase transition to an ice-equivalent solid phase.[7,8] Additional examinations of water in terms of the QCE approach include investigations on isotopically substituted water as well as the influence of quantum chemical methodology on the density of the liquid state.[4,6,9] Besides pure water, the QCE model was furthermore successfully applied to different other associated liquids, for instance, formamide, methanol, ethanol, formic acid, and liquid sulfur, to name but a few.[10−15] More recent investigations concern the importance of the tetrahedral coordination in liquid water for the reproduction of its anomalous properties as well as the influence of cooperative and dispersion effects in liquid *cis*,*cis*-cyclotriazane.[16,17] These studies suggest that the cluster approach is a reliable approximation to the thermodynamics of the condensed phase, at least in the case of highly associated liquids. As already mentioned, the two most crucial points in the QCE procedure are the approximate treatments of intercluster interaction and excluded volume. Due to these corrections, the aforementioned ideal cluster gas in a sense becomes a real (that is condensed) cluster gas, in which the constituents exhibit an appropriate volume and are allowed to interact with each other. The isolated cluster structures obtained from the static quantum chemical calculations are embedded in an attractive mean field potential, which models the dense character of associated liquids and which is the reason why QCE calculations clearly have to be distinguished from cluster studies in which isolated cluster entities are applied. Thus, the present QCE approach can be understood as the first step toward the answer to the legitimate question of what clusters can tell us about the condensed phase.

In the present study we introduce only slightly larger water clusters compared to those investigated previously[4,6] to pronounce the effect due to the tetrahedral coordination and not due to more compact or much larger structures. However, these new clusters contain rings interconnected via a tetrahedrally coordinated water molecule, and we present results of electronic structure calculations with explicit correlation, i.e., Møller−Plesset perturbation theory (MP2). The Results start with improved accuracies for the old (**2/3**) cluster set formerly denoted as the **7(w8cube)** cluster set.[4,6] This part is followed by a comparison of isobars including and excluding the new tetrahedrally coordinated water molecules. We determine optimal cluster sets with respect to the calculated isobars ($\mathbf{2_{opt}}$ = old optimized and $\mathbf{2-4_{opt}}$ = new optimized) by deleting underpopulated clusters. The optimization of a cluster set as the basis for the QCE calculation is thereby examined in detail. Furthermore, we analyze the liquid-phase composition in terms of monomer-normalized populations. Next, we study dispersion versus cooperative effects at constant parameters, and we discuss the different water model structures and the shortcomings of theoretical investigations. The present paper ends with the Conclusion.

## 2. Methodology

**2.1. Quantum Cluster Equilibrium Details.** A full derivation of the QCE theory can be found elsewhere.[3,4,6] The most important aspects of the QCE method are given in the following.

*2.1.1. Partition Functions.* Neglecting vibrational−rotational interactions and other small perturbations, the cluster partition function can be factorized into the translational ($q_{j,\mathrm{trans}}$), vibrational ($q_{j,\mathrm{vib}}$), rotational ($q_{j,\mathrm{rot}}$), and electronic ($q_{j,\mathrm{elec}}$) contributions in the usual way, resulting in

$$q_j = q_{j,\mathrm{trans}} q_{j,\mathrm{vib}} q_{j,\mathrm{rot}} q_{j,\mathrm{elec}} \tag{1}$$

In the high-temperature continuum limit the translational partition function is given by

$$q_{j,\mathrm{trans}} = \frac{V - V_{\mathrm{excl}}}{\Lambda_j^{\,3}} \tag{2}$$

Here $\Lambda_j$ is the thermal de Broglie wavelength in one dimension

$$\Lambda_j = \frac{h}{(2\pi m^{(j)} k_{\mathrm{B}} T)^{1/2}} \tag{3}$$

with $m^{(j)}$ being the mass of cluster $j$, $h$ the Planck constant, $T$ the temperature, and $k_{\mathrm{B}}$ the Boltzmann constant. The numerator of eq 2 describes the available volume for free translational motion. This free volume is obtained by subtracting an excluded volume proportional to the total molecular volume of all clusters from the phase volume

$$V_{\mathrm{exc}} = b_{\mathrm{xv}} \sum_{j=1}^{\eta} n_j V_j \tag{4}$$

where the proportionality constant $b_{\mathrm{xv}}$ serves as one of two variable parameters to adjust the calculations to experimental data. The rotational partition function $q_{j,\mathrm{rot}}$ is also deduced from the continuum limit as

$$q_{j,\mathrm{rot}} = \frac{1}{\sigma}\left(\frac{\pi T^3}{\Theta_{\mathrm{A}}\Theta_{\mathrm{B}}\Theta_{\mathrm{C}}}\right)^{1/2} \tag{5}$$

with the rotational symmetry factor $\sigma$ derived from the optimized cluster structure and the rotational temperatures represented by $\Theta_{\mathrm{A}}$, $\Theta_{\mathrm{B}}$, and $\Theta_{\mathrm{C}}$. These can be calculated from the three principle rotation axes achieved from the

calculated moments of inertia $I_A$, $I_B$, and $I_C$ of a given cluster by following the equation

$$\Theta_X = \frac{\hbar^2}{2I_X k_B} \tag{6}$$

with X = A, B, or C. The next term gives the vibrational contribution $q_{j,vib}$. For each of the $3N - 6$ normal modes, with $N$ being the number of atoms in the molecule, the harmonic oscillator approximation is employed, resulting in

$$q_{j,vib} = \prod_{n=1}^{3M_j-6} (e^{-\Theta_n^{(j)}/2T})(1 - e^{-\Theta_n^{(j)}/T})^{-1} \tag{7}$$

with $M_j = 3i_j a$ as the number of atomic nuclei in cluster $j$ with $a$ atoms per monomer $i$ and the vibrational temperature represented by $\Theta_n^{(j)}$

$$\theta_n^{(j)} = \frac{h\nu_n^{(j)}}{k_B} \tag{8}$$

which is associated with the vibrational frequency $\nu_n^{(j)}$ of the $n$th normal mode. In eq 7 the zero-point vibrational energy (ZPVE) is taken into account by the $e^{-\theta_n^{(j)}/2T}$ term. The treatment of this nuclear quantum effect is not included in every method; for example, most molecular dynamics simulations neglect this contribution.[18]

The last contribution to the canonical partition function is a modified electronic part, depending on the cluster interaction energies of the different species.[3] Therefore, the zero point of the energy scale is set to the total ground-state energy of the relaxed monomer $E_1$. The cluster interaction energy includes on one hand the important nonpairwise additive cooperative effects and on the other hand, according to the used electronic structure method, dispersion effects. Additionally, pairwise additive interaction energies obtained in the way described in ref 6 were applied to this contribution instead of the total cooperative energies. At this point it should be mentioned that the cluster interaction energies ($\Delta E_j^{cp} = E_j^{cp} - i_j E_1$) were always corrected by employing a full counterpoise correction as introduced by Boys and Bernardi.[19]

Here higher contributions than the electronic ground state are neglected. Up to this point only intracluster interaction energies were taken into account. To treat the attractive intercluster interaction energies as well, the volume- and cluster-size-dependent mean field potential energy

$$E_j^{inter} = -i_j a_{mf} V^{-1} \tag{9}$$

was introduced to the model, containing the mean field parameter $a_{mf}$.[3] Finally, the complete electronic contribution to the partition function reads

$$q_{j,elec} = e^{[\Delta E_j^{cp} + E_j^{inter}]/k_B T} \tag{10}$$

*2.1.2. Equilibrium and the Polynomials.* The QCE method assumes a thermodynamic equilibrium between differently sized clusters and one corresponding reference cluster. The largest possible number of monomers $\xi_\eta$ of the largest cluster $X_n$ in this equilibrium may be different from the total number of clusters $\eta$. Following from this, the number of monomers $i_j$ in a given cluster and the "list" number $j$ of that cluster can be different. Thus, the equilibrium reads

$$X_1 \leftrightarrows \frac{X_2}{2} \leftrightarrows \frac{X_3}{3} \leftrightarrows \frac{X_4}{4} \leftrightarrows \ldots \leftrightarrows \frac{X_j}{i_j} \leftrightarrows \ldots \leftrightarrows \frac{X_\eta}{\xi_\eta} \tag{11}$$

Here $X_j$ denotes a cluster of $i_j$ monomer units up to $\xi_\eta$ monomer units forming the largest cluster. $\eta$ represents the total number of clusters. Using the relation between the cluster partition function $q_j$ and the chemical potential $\mu_j$ for which the same equilibrium holds as in eq 11

$$\mu_j = -k_B T \ln\left(\frac{q_j}{N_j}\right) \tag{12}$$

and assuming particle conservation

$$N_A = N_1 + 2N_2 + 3N_3 + 4N_4 + \ldots + i_j N_j + \ldots + \xi_\eta N_\eta \tag{13}$$

leads per insertion of eq 12 into eq 13 to an iterative cycle for the root finding of the population polynomial and the volume polynomial.[6] $N_A$ denotes the Avogadro number and $N_j$ the particle number. Changing to moles $n_j = N_j/N_A$ instead of particle numbers, the population polynomial for the monomer (with the partition function $q_1$) is given by the following expression:

$$0 = -1 + \sum_{j=1}^{\eta} \left[\frac{i_j q_j (N_A)^{i_j - 1}}{(q_1)^{i_j}}\right] (n_1)^{i_j} \tag{14}$$

In a similar manner one arrives at the volume polynomial:

$$0 = -pV^3 + [RT\sum_{j=1}^{\eta} n_j + pV_{excl}]V^2 - [\sum_{j=1}^{\eta} i_j n_j a_{mf}]V + [\sum_{j=1}^{\eta} i_j n_j a_{mf}]V_{excl} \tag{15}$$

$R$ is the ideal gas constant, and $p$ is the chosen pressure. The degree of the volume polynomial depends on whether the mean field interaction is employed ($a_{mf} \neq 0$) or not ($a_{mf} = 0$). From quantum chemical calculations the input for the partition functions is obtained. These will be described in the next section in brief. The partition functions will next serve in the polynomial equations, which leads to different sets of populations and volumes. From these sets the one combination with minimal Gibbs energy is chosen, and this volume/population combination is re-entered into the iterative cycle until volume convergency is reached.

**2.2. Computational Details.** It is important to repeat that inherent to the QCE model we define two interaction terms: First is the *intercluster* interaction, which is the interplay between different clusters; see also section 2.1.1. In the QCE model this interaction is accounted for by a mean field energy term depending on the mean field parameter $a_{mf}$.[3,7] Second is the *intracluster* interaction, which represents the binding energy of a single cluster and which is

$$\Delta E_j^{cp} = E_j^{cp} - i_j E_1 \quad (16)$$

where $E_j$ and $E_1$ denote the total energies of the $j$th cluster containing $i_j$ monomers and the corresponding monomer in its relaxed geometry (adiabatic interaction energy). It is obvious that the *intercluster* term containing $a_{mf}$ accounts for the deficiencies of the cluster approach due to incomplete solvation and that both terms contribute to the condensed-phase behavior.

The pair energies were calculated as described previously.[4,6] All pair energies listed in ref 6 were recalculated. Here only the interaction between each pair in a cluster is considered. Structure optimizations were performed employing density functional theory (DFT) as well as second-order Møller−Plesset perturbation theory (MP2) with the resolution of identity (RI) procedure.[20] The program packages used for the electronic structure calculations were Turbomole 5.91 and associated programs.[20] For DFT calculations, the gradient-corrected functional BP86 was employed in combination with the TZVP and TZVPP basis sets as well as the RI technique. The MP2 calculations were additionally carried out with the TZVP and TZVPP basis sets.[20] As stated above, the basis set superposition error is treated in terms of the counterpoise correction of Boys and Bernardi.[19] For the determination of the principal moments of inertia and the harmonic frequencies, the SNF program package was employed after the electronic structure calculations were carried out.[21] The SNF program computes frequencies on the basis of the harmonic approximation as numerical derivatives of the analytic gradients provided by the structure optimization routine. All harmonic frequencies enter the vibrational partition function unscaled. The two parameters of the QCE model are adjusted to reproduce experimental volumes[22] only and not to reproduce other quantities. Once the parameters are chosen, they are fixed for the calculation of other quantities.

The QCE calculations were performed employing the PEACEMAKER code.[23] To obtain optimal values for the excluded volume and mean field interaction parameters, a sampling of isobars over a predefined $a_{mf}/b_{xv}$ interval is carried out, and the "best choice" isobar with respect to the experimental curve is determined. The employed selection procedure is a straightforward application of the commonly used least-squares fit and is described elsewhere.[5] Within this work we adjusted $a_{mf}$ and $b_{xv}$ to achieve the accuracy $||\Delta V||$ to the fourth decimal place, which equates to a magnitude of microliters.

## 3. Cluster Sets Investigated

To conduct our study on liquid water, we used the cluster set as introduced in the first publication of Weinhold[3,7] and as employed previously by the present authors;[4−6] see Figure 1. The original **2/3** cluster set (formerly denoted as the **7(w8cube)** set)[4−6] mainly contains structural motifs of a 2-fold coordinated water molecule with as many acceptor−donor (AD) hydrogen bonds as water molecules in the cluster. Only in the **w8cube** (which replaced the ringlike **w8** cluster,[4−6] because the **w8** ring was not found to be a minimum for the MP2 method) is at least a 3-fold coordination provided with four ADD and four AAD coordinated molecules.

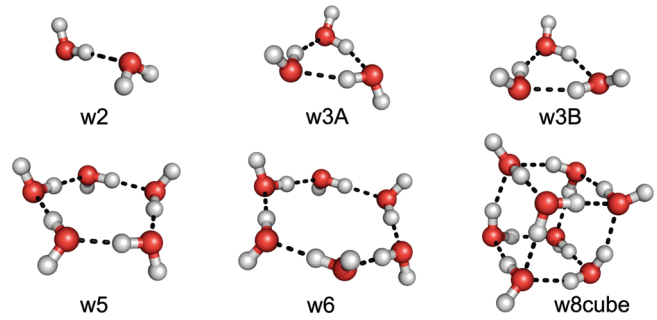


***Figure 1.*** Ball-and-stick model of the original cluster set (abbreviated as the **2/3** set) as introduced by Weinhold[3,7] and as employed previously by the present authors.[4−6]

***Table 1.*** Adiabatic Interaction Energies $\Delta E_j$ and Negative Energies per Monomer $-\Delta E_j/i_j$ (kJ/mol) from Refs 4 and 6[a]

| | BP | | MP2 | | |
|---|---|---|---|---|---|
| | TZVP | TZVPP | TZVP | TZVPP | |
| cluster $j$ | cooperative | cooperative | cooperative | cooperative | pair |
| | | | $\Delta E_j$ | | |
| **w2** | −20.9 | −18.0 | −19.9 | −19.2 | −19.0 |
| **w3A** | −68.5 | −61.4 | −60.3 | −61.7 | −46.4 |
| **w3B** | −63.9 | −57.3 | −57.3 | −58.6 | −44.0 |
| **w5** | −162.3 | −147.9 | −140.4 | −140.9 | −68.2 |
| **w6** | −201.4 | −182.5 | −175.2 | −175.0 | −74.3 |
| **w8cube** | −311.9 | −283.0 | −269.9 | −280.9 | −98.4 |
| | | | $-\Delta E_j/i_j$ | | |
| **w2** | 10.5 | 9.0 | 10.0 | 9.6 | 9.5 |
| **w3A** | 22.8 | 20.5 | 20.1 | 20.6 | 15.5 |
| **w3B** | 21.3 | 19.1 | 19.1 | 19.5 | 14.7 |
| **w5** | 32.5 | 29.6 | 28.0 | 28.2 | 13.6 |
| **w6** | 33.6 | 30.4 | 29.2 | 29.2 | 12.4 |
| **w8cube** | 39.0 | 35.4 | 33.7 | 35.1 | 12.3 |
| | | | $-\Delta E_j/n^{hb}$ | | |
| **w2** | 20.9 | 18.0 | 19.9 | 19.2 | 19.0 |
| **w8cube** | 26.0 | 23.6 | 22.5 | 23.4 | 8.2 |

[a] The last two lines give the negative energy per hydrogen bond ($n^{hb}$), which is different for the dimer and the **w8cube** cluster only.

In Table 1 we list the interaction energies and the negative energies per monomer for the **2/3** cluster set. For all methods and basis sets employed **w8cube** is the most stable cluster followed by the **w6** and **w5** clusters. In the pair energies per monomer (second block, last column, Table 1) these trends are not present. Although **w2** is still the least stable cluster, it is followed by the **w8cube** and **w6** clusters. Thus, in **w6** and **w8cube** we observe large cooperative effects.

To probe the 4-fold coordination, further clusters were added; see Figure 2. We call these additional clusters "spiro clusters'' to illustrate the analogy to organic spiro compounds. A further feature of the spiro clusters next to the structural motif of the 4-fold coordination is that they are larger than most of the clusters from the **2/3** set. The leading structural motif in all spiro clusters is one AADD water molecule and $i_j - 1$ molecules with AD hydrogen bonds per water molecule. The combination of these new spiro-type clusters and the members of the old **2/3** set will be called **2−4** set. The interaction energies together with the energies per monomer and per hydrogen bond and the basis set

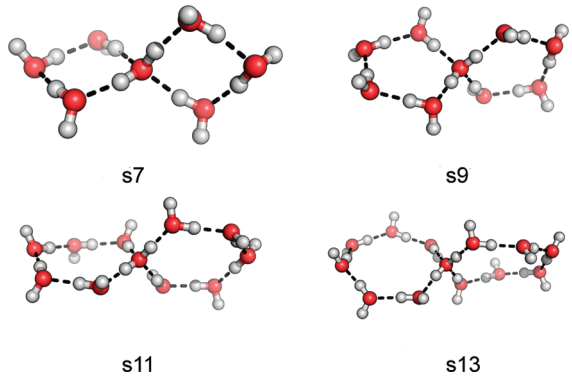


***Figure 2.*** Ball-and-stick model of additional clusters.

***Table 2.*** Adiabatic Interaction Energies $\Delta E_j$, BSSEs, Negative Energies per Monomer $-\Delta E_j/i_j$, and Negative Energies per Hydrogen Bond $-\Delta E_j/n^{hb}$ (kJ/mol)

| | BP | | MP2 | | |
|---|---|---|---|---|---|
| | TZVP | TZVPP | TZVP | TZVPP | |
| cluster $j$ | cooperative | cooperative | cooperative | cooperative | pair |
| | | | $\Delta E_j$ | | |
| **s7** | −247.3 | −218.6 | −203.1 | −208.8 | −90.6 |
| **s9** | −324.7 | −296.5 | −279.9 | −281.7 | −75.0 |
| **s11** | −392.5 | −356.3 | −342.5 | −342.8 | −66.5 |
| **s13** | −461.6 | −416.6 | −405.2 | −402.8 | −52.1 |
| | | | BSSE | | |
| **s7** | −24.6 | −24.6 | −56.0 | −40.4 | −307.6 |
| **s9** | −44.1 | −31.5 | −75.4 | −53.4 | −101.3 |
| **s11** | −54.3 | −38.4 | −91.4 | −63.8 | −102.8 |
| **s13** | −62.2 | −43.7 | −104.8 | −72.6 | −212.8 |
| | | | $-\Delta E_j/i_j$ | | |
| **s7** | 35.3 | 31.2 | 29.0 | 29.8 | 12.9 |
| **s9** | 36.1 | 32.9 | 31.1 | 31.3 | 8.3 |
| **s11** | 35.7 | 32.4 | 31.1 | 31.2 | 6.0 |
| **s13** | 35.5 | 32.1 | 31.2 | 31.0 | 4.0 |
| | | | $-\Delta E_j/n^{hb}$ | | |
| **s7** | 30.9 | 27.3 | 25.4 | 26.1 | 11.3 |
| **s9** | 32.5 | 29.7 | 28.0 | 28.2 | 7.5 |
| **s11** | 32.7 | 29.7 | 28.5 | 28.6 | 5.5 |
| **s13** | 33.0 | 29.8 | 28.9 | 28.8 | 3.7 |

superposition errors for different methods and basis sets are listed in Table 2.

Employing a larger basis set (TZVPP instead of TZVP) leads to a decrease of the absolute values of the interaction energies for the density functional methods and to an increase of the absolute values of interaction energies in the case of MP2, with the exception of **s13**. The basis set superposition errors (BSSEs) are in the range of 20−100 kJ/mol, depending on the method and basis set as well as the cluster size. As can be expected, the BSSEs decrease with increasing basis set. Considering the energies per monomer, we find that within a chosen basis set and method the energies are all similar, i.e., around 36 kJ/mol for BP/TZVP, 32 kJ/mol for BP/TZVPP, and around 31 kJ/mol for the MP2 calculations. Thus, these clusters are all more stable than those from the **2/3** cluster set with the exception of the **w8cube**; see Table 1. Again the pair energies reverse trends, showing that large cooperative effects do play a role. Due to their geometrical conformation, the spiro clusters show a higher cooperativity on average; i.e., they have smaller pair energies than the clusters from the old **2/3** set. Considering the energy per hydrogen bond, it is obvious why the **w5** and **w6** clusters are such important structures for the liquid phase, because these clusters are those with the strongest hydrogen bonds on average. However, the spiro clusters are only a little less stable than the **w6** cluster. As can be observed from the last block of Table 2, these kinds of clusters provide average hydrogen bonds as strong as those of the **w5** cluster and almost as strong as those of the **w6** cluster. In general, we observe the known overbinding of DFT;[24] e.g., for small basis sets BP always leads to stronger bound clusters.

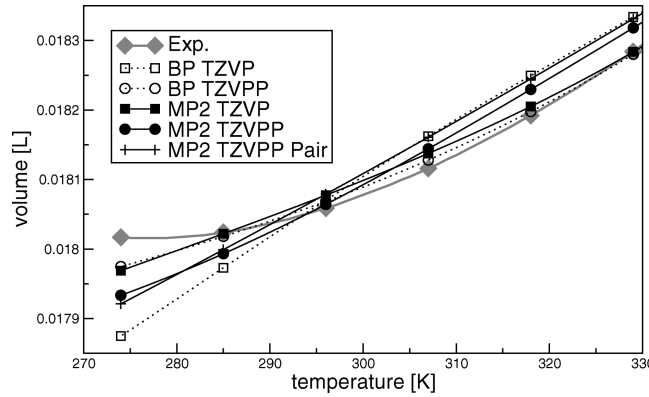


***Figure 3.*** Calculated isobars for the **2/3** cluster set displayed at a temperature range of 274−329 K. For each electronic structure method $a_{mf}$ and $b_{xv}$ are newly adjusted (range 274−373 K); for the results see Table 3.

The corresponding frequency calculations contain only positive values, indicating that we are dealing with minimum structures. For the sake of reproducibility these data can be obtained upon request from the authors.

## 4. Results

**4.1. 2/3 Set: Isobars Revisited and Optimal Set.** We start this section with the newly obtained isobars for the original **2/3** cluster set, i.e., without applying the spiro clusters. The isobars are illustrated in Figure 3. In this figure two electronic structure methods (BP, MP2) and two basis sets (TZVP, TZVPP) as well as MP2/TZVPP pair energies were considered for the selection procedure. It can be recognized that BP/TZVPP follows the experimental curve closest, while BP/TZVP leads to the worst agreement with the experimental data.[22] The MP2 data represent a more accurate electronic structure, because the method treats the electron−electron correlation in higher detail than density functional theory based on the generalized gradient approximation. This does not necessarily lead to the best isobars when the model-inherent parameters of the QCE calculations are allowed to vary. Thus, it is difficult to discuss trends at "improved" electronic structure methods. Interestingly, we obtain different trends for the varying electronic structure methods if we compare the low temperature range and high temperature range. Furthermore, it is evident that the deviations from the experimental isobar at lower temperatures are larger for all methods than at higher temperature. From this behavior the first implications of the importance of the tetrahedral coordination pattern at lower temperatures can be drawn.

***Table 3.*** QCE Parameters for Different Methods and Basis Sets without Spiro Clusters (**2/3** Set) in the Temperature Range from 274 to 373 K[a]

| method | basis set | $\|\|\Delta V\|\|$ | $a_{mf}$ | $b_{xv}$ |
|---|---|---|---|---|
| BP | TZVP | 523.56 | 0.121 | 1.084 |
| BP | TZVPP | 135.49 | 0.158 | 1.110 |
| MP2 | TZVP | 175.05 | 0.162 | 1.099 |
| MP2 | TZVPP | 311.80 | 0.162 | 1.107 |
| MP2 Pair | TZVPP | 445.76 | 0.370 | 1.078 |

[a] $||\Delta V||$ ($\mu$L) gives the accuracy of the selected isobar, i.e., the root mean square deviation from the experimental values.

***Table 4.*** QCE Parameters for MP2/TZVPP Calculations without Spiro Clusters (**2/3** and $\mathbf{2_{opt}}$) and with the Spiro Clusters (**2**−**4** and $\mathbf{2-4_{opt}}$) in the Temperature Range from 274 to 373 K[a]

| set | $\|\|\Delta V\|\|$ | $a_{mf}$ | $b_{xv}$ |
|---|---|---|---|
| **2/3** | 311.80 | 0.162 | 1.107 |
| $\mathbf{2_{opt}}$ | 167.57 | 0.136 | 1.088 |
| **2**−**4** | 166.42 | 0.125 | 1.105 |
| $\mathbf{2-4_{opt}}$ | 137.07 | 0.130 | 1.105 |

[a] $||\Delta V||$ ($\mu$L) gives the accuracy, i.e., the root mean square deviation, from the experimental values.

In the present work we selected the QCE parameters with one more decimal place as in previous studies, which improves in some cases the accuracy by 50%.[5,6] In Table 3 we show the accuracies of the selected QCE parameters for the different electronic structure methods used within this work. The same trends in the value of the accuracy $||\Delta V||$ as those discussed for the plots of Figure 3 can be observed in Table 3. A highly intuitive point of the QCE model is that the smaller the intracluster interaction energies are, the larger the parameter accounting for the mean field interaction $a_{mf}$ becomes. This demonstrates that the parameter in a way accounts for the deficiencies of the missing interactions, whether arising from the intercluster part or not treated correctly by the electronic structure method (for instance, overestimated for BP/TZVP). This point is most striking for the pair energies where the $a_{mf}$ value is more than twice as large as the $a_{mf}$ value of the corresponding MP2/TZVPP QCE calculation. We will discuss this topic of neglected cooperativity in a later section. $a_{mf}$ deviates from that of the uncorrected model ($a_{mf} = 0$ and $b_{excl} = 1$) by up to 0.37 which correspond to 37%, and $b_{xv}$ only varies within 11%, again indicating the pronounced importance of the overall interparticle interactions for the treatment of condensed-phase phenomena.

*4.1.1. Pure 2-Fold Coordinated Cluster Set and Monomer-Normalized Populations.* To examine the influence of the different clusters in the set, we determined an optimal set by deleting clusters systematically under the proposition of keeping the same level of accuracy. Initially, we studied the elimination of those clusters that are found to be weakly populated, which led to the exclusion of the **w3B** cluster. Because the aim of the accompanying paper (10.1021/ct900189v) is to investigate the importance of the 2-fold versus the 4-fold coordination, we additionally constructed a set consisting of pure 2-fold hydrogen-bonded motifs. This means that **w8cube** is deleted from the cluster set as well, which leads to an even more accurate isobar for the MP2/TZVPP data, as can be seen in the first two lines of Table 4. The set obtained in this way will be denoted as the $\mathbf{2_{opt}}$ set. The resulting QCE parameters are $a_{mf} = 0.136$ and $b_{xv} = 1.088$, and the accuracy is $||\Delta V|| = 167.57$ $\mu$L, which is even smaller by a factor of 2 as compared to the accuracy of the complete **2/3** set; see Table 3. Interestingly, the $a_{mf}$ value is reduced, which indicates that either the **w3B** or the **w8cube** cluster must have a destabilizing effect on the intercluster interaction. It also indicates that it is mandatory to optimize the cluster set as a basis for the QCE calculation to obtain excellent results. The old (gray) and newly obtained (black) cluster populations are shown on the left side of Figure 4. While only slight changes in the high-temperature region can be recognized (see the gray curves with squares in Figure 4, left panel) the **w6** cluster becomes the most important cluster at lower temperature (see the black curves with circles in Figure 4, left panel). The **w5** cluster population also increases a little bit at lower temperature as compared to the behavior in the **2/3** set. This is in accordance with the isolated molecule energetics formerly discussed in section 3. On the right-hand side of Figure 4 we show the monomer-normalized populations which will be used in the accompanying paper (10.1021/ct900189v), because they provide a more physical picture of the particular phase point. The cluster populations on the left side of Figure 4 refer to the total number of clusters composing the actual phase point, but this amount varies within each step of the QCE calculation. This means that if mainly large clusters are populated, more monomers are bound within these large clusters. Because the amount of monomers is fixed in the QCE calculation, there are fewer monomers to form the other clusters. This implies a reduction of the total number of clusters; i.e., if the total number of clusters decreases, the population of each individual cluster increases. Thus, for our purpose it is better to analyze monomer-normalized populations (see the right side of Figure 4), which are applied in the monomer reference system. For all phase points the total number of monomers is equal to 1 mol. The percentage now indicates how many of the total 1 mol monomers are bound in a particular cluster and thereby reflects the physical composition of the phase point. From Figure 4, right panel, we observe that the liquid phase of the $\mathbf{2_{opt}}$ set is almost completely composed of the **w6** cluster and the **w5** cluster. While the **w6** population decreases from 79% to approximately 63%, the **w5** population grows from 20% to 29% with increasing temperature.

**4.2. 2−4 Cluster Set and Optimal $\mathbf{2-4_{opt}}$ Cluster Set.** We now turn to the larger cluster set containing tetrahedrally coordinated water molecules, namely, the **2**−**4** cluster set. The obtained parameters and accuracies are listed in Table 4. The data clearly demonstrate that the inclusion of the spiro clusters leads to an improvement in the accuracy over that of the **2/3** cluster set. Interestingly, the $a_{mf}$ value of the **2**−**4** set is reduced as compared to that of the **2/3** set. This is not a general rule; see Table 3. Here a better accuracy goes along with smaller and in some cases with larger $a_{mf}$ values. However, from this observation we can deduce that the tetrahedrally coordinated water molecule in the particular

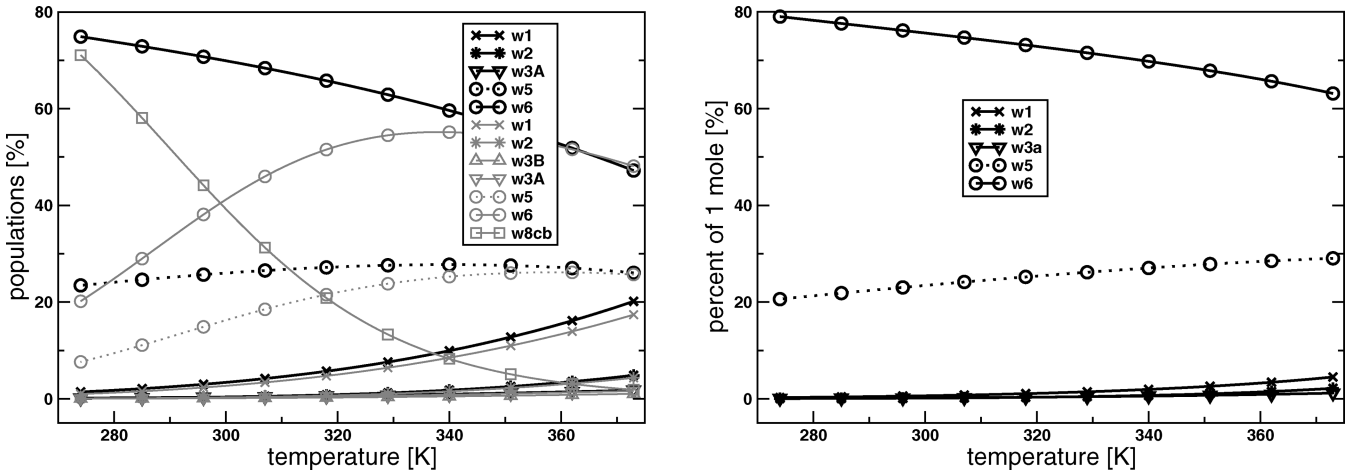


***Figure 4.*** Obtained populations for the **2/3** cluster set (gray) and the $\mathbf{2}_{opt}$ cluster set (black) at the temperature range of 274−373 K for MP2/TZVPP: left, cluster populations; right: monomer-normalized populations. The QCE parameters are $a_{mf} = 0.136$ and $b_{xv} = 1.088$.

spiro cluster mimics the intercluster interaction more accurately, leading to a reduction of the $a_{mf}$ value.

To examine the influence of the different clusters in the **2**−**4** set, we determine another optimal set (abbreviated as the $\mathbf{2}-\mathbf{4}_{opt}$ set) by systematically deleting clusters under the proposition of keeping the same level of accuracy. Therefore, we studied the elimination of those clusters that were found not to be populated highly, i.e., **w3A**, **w3B**, **s7**, and **s13**. Their elimination leads in some cases to similar results, but in nearly half the possibilities to slightly improved results as compared to taking the whole cluster set into account, which is shown in Table 6 in the Appendix. Thus, the $\mathbf{2}-\mathbf{4}_{opt}$ cluster set contains the old clusters **w1**, **w2**, **w3B**, **w5**, **w6**, and **w8cube** as well as the new **s9** and **s11** clusters. In Table 4 the results of the selection routine are also given for the $\mathbf{2}-\mathbf{4}_{opt}$ set. Again $a_{mf}$ is reduced compared to that of the $\mathbf{2}_{opt}$ set, although only to a small extent. The QCE parameters are almost identical to those obtained for the complete set; see Table 4. What is also apparent from Table 4 is that the addition of clusters containing tetrahedrally coordinated water leads to a strong improvement of the accuracy; compare values for the **2/3** set with those for the **2**−**4** set or values for $\mathbf{2}_{opt}$ with those for the $\mathbf{2}-\mathbf{4}_{opt}$ set. Both quantities, the accuracy and $a_{mf}$, point to a better description of liquid water when tetrahedrally coordinated molecules are present. This will be discussed in more detail in the accompanying paper (10.1021/ct900189v).

**4.3. Constant Parameters and Varying Electronic Structures.** After definition of an optimal cluster set ($\mathbf{2}-\mathbf{4}_{opt}$), isobars are calculated at constant QCE parameters for all used electronic structure methods and their corresponding frequencies in this section. The results are shown in Figure 5. At higher temperature larger deviations from the experimental isobar can be observed. Again there are trends for the different electronic structure methods. The BP method with TZVP and TZVPP yields the highest intracluster interaction energies, which is reflected in small volumes. However, according to the larger energies found for BP/TZVP, smaller volumes than for the BP/TZVPP calculations would be expected, but the opposite trend is observed. This clearly shows the important influence of the other two

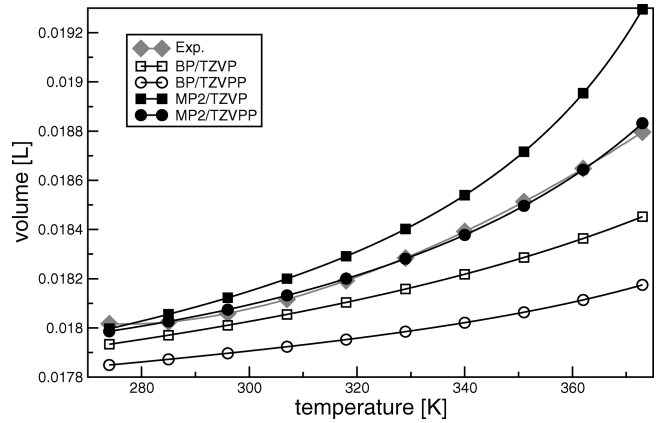


***Figure 5.*** Isobars at the liquid-phase temperature range for the $\mathbf{2}-\mathbf{4}_{opt}$ set with $a_{mf} = 0.130$ and $b_{xv} = 1.105$.

partition functions, i.e, the rotational and the vibrational contributions, which in some cases disturb the reciprocally proportional relation between interaction energy and volume. According to Table 2, MP2/TZVP calculations lead to the smallest intracluster interaction energies; thus, the volumes are much larger than for the other methods.

To study the pure influence of the electronic structure method and the electronic partition function, we computed isobars at constant input for the rotational and vibrational partition functions and applied constant QCE parameters; see Figure 6. Because the MP2/TZVPP set parameters were adjusted to the experimental curve, we observe an excellent agreement between MP2/TZVPP and the experimental isobar. The MP2/TZVP curve deviates now much less as compared to the results depicted in Figure 5, indicating again the strong influence of the vibrational and rotational partition functions.

All methods show larger deviations at higher temperature. The smallest overall volumes are obtained from the BP/TZVP energies, which predict the strongest binding energies for all clusters compared to the other electronic structure methods. The BP/TZVPP isobar is slightly closer to the experiment. This reflects an interesting and unexpected basis set dependency of DFT and might be important in light of

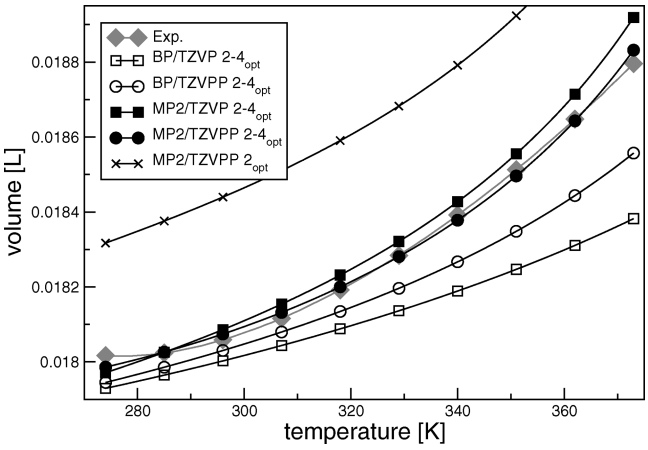


***Figure 6.*** Isobars at the liquid-phase temperature range for the $\mathbf{2-4_{opt}}$ set with $a_{mf} = 0.130$ and $b_{xv} = 1.105$ at constant MP2/TZVPP frequencies and moments of inertia from MP2/TZVPP geometries.

***Table 5.*** QCE Parameters for the TZVPP Basis Set and MP2 Calculations without Spiro Clusters ($\mathbf{2_{opt}}$) and with Spiro Clusters ($\mathbf{2-4_{opt}}$) in the Temperature Range from 274 to 373 K[a]

| set | $\|\|\Delta V\|\|$ | $a_{mf}$ | $b_{xv}$ |
|---|---|---|---|
| $\mathbf{2_{opt}}$ | 167.57 | 0.136 | 1.088 |
| $\mathbf{2_{opt}}$ pair | 405.63 | 0.343 | 1.068 |
| $\mathbf{2-4_{opt}}$ | 137.07 | 0.130 | 1.105 |
| $\mathbf{2-4_{opt}}$ pair | 420.18 | 0.351 | 1.071 |

[a] $\|\|\Delta V\|\|$ ($\mu$L) gives the accuracy, i.e., the root mean square deviation from the experimental values.

the current basis set limit studies of Lee and Tuckerman, who found no glassy or overstructured state in a 60 ps first-principles simulation on water employing the BLYP density functional with a complete discrete variable representation (DVR) basis set.[24] The improved volume at larger basis set in the isobars of the density functional theory compared with the too small volume with small basis set might thus be in accordance with the "unfrozen water state" of the DVR simulation by Lee and Tuckerman.[24] Another interesting feature is the nonconstant deviation between calculated BP data and experimental data. At higher temperature the deviations become much larger due to the wrong slope of the BP isobars. Thus, our data indicate that using density functional theory (BP) as well as a small basis set leads to a less accurate description of the liquid phase especially at high temperature as compared to MP2 with the TZVPP basis set. Because we observe volumes which are too small for the isobars, we can deduce that both approximations could be the origin for an overstructured liquid as discussed by Lee and Tuckerman.[24]

Next, we compare the different monomer-normalized populations of the $\mathbf{2-4_{opt}}$ set, which are depicted in Figure 7. While MP2/TZVPP shows nonlinear curves for the populations of different clusters with varying temperature, the other electronic structure methods lead to a linear behavior for almost all clusters. Both BP electronic structure calculations populate the **s9** cluster far too much if compared to the MP2/TZVPP reference. Furthermore, the **s9** cluster population is still larger than the ring cluster population at high temperature for BP. This result might be comparable to the findings of Shields and Kirschner, who observed that some specific structures if calculated with DFT are not minimum structures.[25] Please note that comparing MP2 populations with large and small basis sets also shows differences.

**4.4. Cooperativity.** For both the $\mathbf{2_{opt}}$ set and the $\mathbf{2-4_{opt}}$ set we again list the accuracy and the QCE parameters in Table 5 together with the results of the pair energies applied to both optimal sets. The derivation of pair energies is described in refs 4 and 6. Comparing the $a_{mf}$ values for both sets obtained with and without inclusion of cooperative effects, we find that $a_{mf}$ increases by a factor larger than 2 for the calculations based on the pair energies. The difference in $a_{mf}$ comparing the two sets is also present if we consider the QCE results obtained from the pair energies. In contrast to the behavior of the cooperative energies, the $a_{mf}$ value for the pair energies (Table 5) is larger for the $\mathbf{2-4_{opt}}$ set than for the $\mathbf{2_{opt}}$ set, corresponding to the fact that cooperative effects in the spiro clusters with tetrahedrally coordinated water are more severe than in the $\mathbf{2_{opt}}$ cluster set.

The pair populations (not depicted) for both optimal sets show a decreasing dimer population from 86% to approximately 27% and an increase in the monomer population with increasing temperature to the extent of 27%, while the larger clusters are not significantly populated at all. Again these findings are comparable to the results obtained by Lee and Tuckerman.[24] The authors compared conditional correlation functions for hydrogen bonds in water as obtained from traditional molecular dynamics simulations with a nonpolarizable model to their first-principles simulations. While the functions decayed for all choices of coordination environment with the same speed in the traditional molecular dynamics simulations, first-principles simulations could show that the function for water with a 4-fold coordination decreases significantly slower, indicating that tetrahedrally coordinated water might possess extra stability.[24]

## 5. Discussion

Reconsidering the hydrogen bond, it is obvious that the strength of the particular hydrogen bond should be an objective. Weak and strong hydrogen bonds per particular water molecule are discussed in an asymmetric model.[26] From the point of view of static calculations we observe that some tetrahedrally coordinated water exhibits asymmetric coordination; i.e., individual hydrogen bonds are of different stabilities. However, if an average is taken over each of the tetrahedrally coordinated water molecules in an ensemble, this could wash out subtle effects, and as a result the four hydrogen bonds would be of similar strength. Interestingly, one of our clusters, namely, **s9**, shows an almost perfectly symmetric central water molecule (NBO[27,28] occupation numbers of each accepting $\sigma^*$ orbital of the four hydrogen bonds, obtained with HF/SVP: 0.036, 0.036, 0.034, and 0.034), while the other spiro clusters deviate much more from perfect symmetry. For example, **s11** shows occupation numbers at the AADD water molecule of 0.035, 0.033, 0.024, and 0.041. It might be important that the **s9** cluster with the closest symmetric coordination plays such a dominant role;

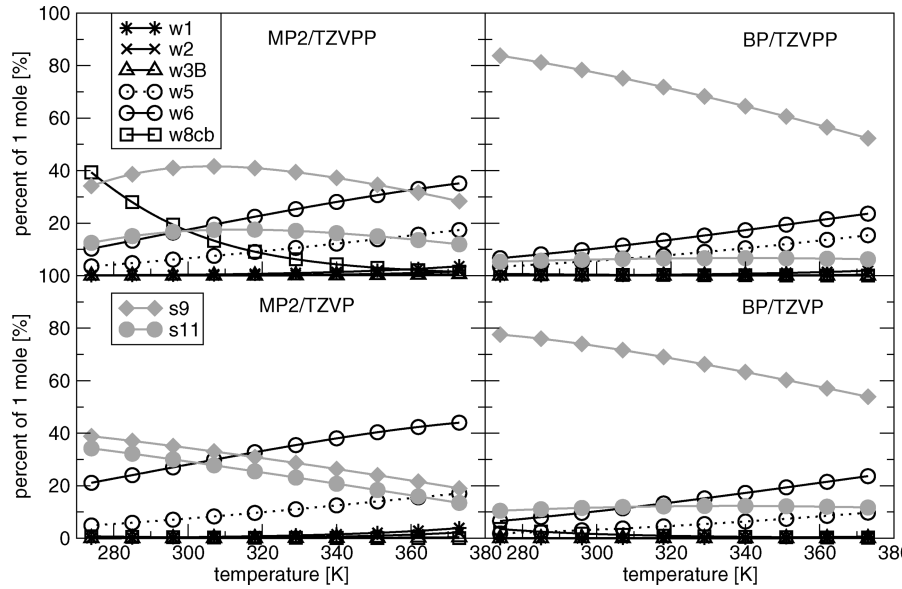


***Figure 7.*** Populations at the liquid-phase temperature range for the **2**−**4**$_{opt}$ set with $a_{mf} = 0.130$ and $b_{xv} = 1.105$ at constant MP2/TZVPP frequencies.

***Table 6.*** Fit for the Elimination of Different Clusters in the Temperature Range from 274 to 373 K[a]

| | deleted? | | | | | | | | | | | | | | | |
|---|---|---|---|---|---|---|---|---|---|---|---|---|---|---|---|---|
| **w3A** | no | yes | yes | yes | **yes** | no | no | no | yes | yes | yes | no | no | no | no | yes |
| **w3B** | no | yes | yes | yes | **no** | yes | no | yes | yes | no | no | yes | no | no | yes | no |
| **s7** | no | yes | yes | no | **yes** | yes | yes | yes | no | yes | no | no | no | yes | no | no |
| **s13** | no | yes | no | yes | **yes** | yes | yes | no | no | no | yes | yes | yes | no | no | no |
| $\|\|\Delta V\|\|$ | 166 | 144 | 164 | 141 | **137** | 145 | 144 | 169 | 157 | 162 | 138 | 144 | 140 | 169 | 165 | 163 |

[a] The accuracy $\|\|\Delta V\|\|$ is given in the last line in dimensions of microliters. The electronic structure method is MP2/TZVPP.

see Figure 7. The highly populated **w6** cluster is perfectly symmetric as well with occupation numbers of 0.034, while the AD water molecules in the spiro clusters show slightly lower occupation numbers.

From static quantum chemical methods information about the hydrogen bond can be obtained. However, these calculations are based on fixed nuclei positions, and a hydrogen bond definition is difficult, because the wave function cannot be unequivocally distributed among the atoms.[29,30] Furthermore, as Lee and Tuckerman put it nicely, "Although reproducing these (binding) energies is important, small clusters do not represent the bulk...", these investigations neglect the condensed-phase environment completely. Nevertheless, interesting analyses such as energy decomposition to determine the origin of hydrogen bonding were carried out.[30,31]

The QCE method[3,4,6,13] applied in this work is based on static cluster calculations neglecting an explicit dynamical behavior as explained in the Introduction. It includes two parameters, $a_{mf}$ and $b_{xv}$, accounting for the missing intercluster interaction and for excluded volume effects. A direct comparison of different electronic structure models is difficult, because of this parametric dependency but also because of the approximations made within the method.[4,6] However, if the parameters together with the input for the other partition functions are kept constant, the influence of different electronic structure methods can be tested. Despite these difficulties, the QCE method has the advantage that it is up to now the only method to incorporate electronic correlation and cooperative effects in a simple way for calculations of the condensed phase. Furthermore, the method in principle covers every temperature and pressure point in phase as long as the approximations made in the model are valid at that state. Due to the analytical form of the QCE partition functions, calculations of partition-function-dependent quantities are easily carried out. Another advantage of the QCE method is that it allows calculation of populations of clusters and thereby determination of which structural motif plays a role in the examined phases.

## 6. Conclusion

We investigated the liquid-phase isobars of water as obtained from the quantum cluster equilibrium method for different electronic structure methods, namely, MP2 and BP, at different basis sets. Two cluster sets were employed, one where no tetrahedrally coordinated water molecule was present (**2/3** set) and one where such motifs were included (**2**−**4** set). Both sets contain the ring motif, but the **2**−**4** set comprises interconnected ring structures of two equally sized rings. If we apply the **2/3** cluster set and allow the two adjusting parameters of the QCE model to vary, we find only slight differences in the isobars between DFT and MP2. Using a smaller basis set leads to worse agreement as compared to using the larger basis set for both methods. Next, we introduced optimal sets by eliminating underpopulated clusters (**2**$_{opt}$ and **2**−**4**$_{opt}$). This seems to be an important step in the QCE procedure, if high accuracy is desired,

because some clusters destabilize the system. One set contained only pure 2-fold coordinated water molecules ($\mathbf{2_{opt}}$). For the **2/3** and the $\mathbf{2_{opt}}$ cluster set we find that a ring consisting of six monomer units plays a dominant role over the whole temperature range, as observed in previous studies.[5,7] Adding the spiro clusters, we find a significant improvement of our calculated data with respect to experiment, especially at low temperature and concerning the slope of the curve. The QCE parameter accounting for the intercluster interactions decreases by adding tetrahedrally coordinated water molecules, indicating the improved description of the liquid phase in terms of intracluster energetics. Keeping all model parameters constant (at the optimized MP2/TZVPP values) and varying only the electronic structure energies, we find large basis set dependencies for the BP methods. Deviations for the different electronic structure methods from the MP2/TZVPP data obtained with the $\mathbf{2-4_{opt}}$ cluster set are now more pronounced at higher temperature.

**Acknowledgment.** This work was supported by the DFG, in particular by the ERA Chemistry Program and by the SPP-1191 Program. Computer time from RZ Leipzig, HLRS Stuttgart, and NIC Jülich are gratefully acknowledged.

**Note Added after ASAP Publication.** This paper was released ASAP on May 13, 2009, with errors in eq 4 and the following line. The correct version was posted on May 19, 2009.

## Appendix

In Table 6 we list the results of all possible reduced combinations. We find a combination where the accuracy is even improved to $1.37 \times 10^{-4}$ L (bold in the table). We will thus work with the set where **w3A**, **s7**, and **s13** are deleted.

### References

(1) Kirchner, B.; Wennmohs, F.; Ye, S.; Neese, F. *Curr. Opin. Chem. Biol.* **2007**, *11*, 134–141.

(2) Spickermann, C.; Felder, T.; Schalley, C. A.; Kirchner, B. *Chem.—Eur. J.* **2008**, *14*, 1216–1227.

(3) Weinhold, F. *J. Chem. Phys.* **1998**, *109*, 367–372.

(4) Kirchner, B. *Phys. Rep.* **2007**, *440*, 1–111.

(5) Spickermann, C.; Lehmann, S. B. C.; Kirchner, B. *J. Chem. Phys.* **2008**, *128*, 244506.

(6) Kirchner, B. *J. Chem. Phys.* **2005**, *123*, 204116.

(7) Weinhold, F. *J. Chem. Phys.* **1998**, *109*, 373–384.

(8) Ludwig, R.; Weinhold, F. *J. Chem. Phys.* **1999**, *110*, 508–515.

(9) Ludwig, R.; Weinhold, F. *Z. Phys. Chem.* **2002**, *216*, 659–674.

(10) Ludwig, R.; Weinhold, F.; Farrar, T. C. *J. Chem. Phys.* **1995**, *103*, 3636–3642.

(11) Ludwig, R.; Weinhold, F.; Farrar, T. C. *J. Chem. Phys.* **1997**, *107*, 499–507.

(12) Ludwig, R. *ChemPhysChem* **2005**, *6*, 1376–1380.

(13) Borowski, P.; Jaroniec, J.; Janowski, T.; Woliński, K. *Mol. Phys.* **2003**, *101*, 1413–1421.

(14) Wendt, M. A.; Weinhold, F.; Farrar, T. C. *J. Chem. Phys.* **1998**, *109*, 5945–5947.

(15) Ludwig, R.; Behler, J.; Klink, B.; Weinhold, F. *Angew. Chem., Int. Ed.* **2002**, *41*, 3199–3202.

(16) Ludwig, R. *ChemPhysChem* **2007**, *8*, 938–943.

(17) Song, H.-J.; Xiao, H.-M.; Dong, H.-S.; Huang, Y.-G. *J. Mol. Struct.: THEOCHEM* **2006**, *767*, 67–73.

(18) Huber, H.; Dyson, A.; Kirchner, B. *Chem. Soc. Rev.* **1999**, *28*, 121–133.

(19) Boys, S. F.; Bernardi, F. *Mol. Phys.* **1970**, *19*, 553–566.

(20) Ahlrichs, R.; Bär, M.; Häser, M.; Horn, H.; Kölmel, C. *Chem. Phys. Lett.* **1989**, *162*, 165–169.

(21) Neugebauer, J.; Reiher, M.; Kind, C.; Hess, B. A. *J. Comput. Chem.* **2002**, *23*, 895–910.

(22) Lemmon, E. W.; McLinden, M. O.; Friend, D. G. Thermophysical Properties of Fluid Systems. In *NIST Chemistry WebBook, NIST Standard Reference Database Number 69* [Online]; Linstrom, P. J., Mallard, W. G., Eds.; National Institute of Standards and Technology: Gaithersburg, MD. http://webbook.nist.gov (accessed 2005).

(23) Kirchner, B.; Spickermann, C. *PEACEMAKER*, V1.4 2004-2008; Institute of Physical and Theoretical Chemistry, University of Bonn: Bonn, Germany; Wilhelm-Ostwald Institute of Physical and Theoretical Chemistry, University of Leipzig: Leipzig, Germany, 2008.

(24) Lee, H.; Tuckerman, M. E. *J. Chem. Phys.* **2007**, *126*, 164501.

(25) Shields, G. C.; Kirschner, K. N. *Synth. React. Inorg., Met.-Org., Nano-Met. Chem.* **2008**, *38*, 32–39.

(26) Soper, A. K. *J. Phys.: Condens. Matter* **2005**, *17*, 3273–3282.

(27) Weinhold, F. *Adv. Protein Chem.* **2006**, *72*, 121–155.

(28) Reed, A. E.; Curtiss, L. A.; Weinhold, F. *Chem. Rev.* **1988**, *88*, 899–926.

(29) Reiher, M.; Kirchner, B. *J. Phys. Chem. A* **2003**, *107*, 4141–4146.

(30) Thar, J.; Kirchner, B. *J. Phys. Chem. A* **2006**, *110*, 4229–4237.

(31) Morokuma, K. *Acc. Chem. Res.* **1977**, *10*, 294–300.

CT800310A